Kwasu Function: A Closed-Form Analytical Solution to the Complete Three-Dimensional Unsteady Compressible Navier-Stokes Equation

Taofiq O. Amoloye*

Georgia Institute of Technology, Atlanta, GA, 30332, US

An attempt is made to refine the classical potential theory of the flow over a circular cylinder by introducing a viscous sink-source-vortex sheet on the surface of the cylinder. These singularities introduced into the flow are modeled as concentric at every location. The vortices are modeled as variations of Lamb-Oseen, Batchelor and Burgers vortices and analytic expressions for their strengths and those of the sinks/sources are obtained from the classical theory. These are employed to obtain a viscous potential function named the *Kwasu* function which provides a closed form analytic solution to the complete three dimensional unsteady compressible Navier-Stokes equation. Preliminary results of the work show that the theory presented captures important features of a bluff body flow including flow separation, wake formation, vortex shedding as well as compressibilty effects.The condition at a viscous wall is shown to be transient from slip towards a complete no-slip for a steady freestream flow. It is the hope that the present theory will shed more light on the important phenomenon of turbulence in planned future work in which quantitative analysis of the theory will be carried out.

Nomenclature

a	Speed of sound, Semi-major axis of an ellipse aligned along the body x-axis
$\mathbf{a}$	Acceleration vector
A	Arbitrary constant
b	Semi-minor axis of an ellipse aligned along the body y-axis
B	Arbitrary constant
D	Diameter of cylinder
f	Reynolds number based on cylinder diameter,$f = \frac{V_\infty D}{\nu}$
$\mathbf{g}$	Body force vector
G	Universal gravitational constant
$h, \mathbf{h}$	Specific angular momentum, Specific angular momentum vector
H	Altitude of the center of gravity of a body above a planetary surface
i, j	Indices
k	Doublet strength, Thermal conductivity
m, n	Positive non-zero integers
m	Meter
M	Mach number
$\mathcal{M}$	Mass
p	Pressure
$\mathbf{Q}$	Euler angle transformation matrix
$r, \mathbf{r}$	Radial Coordinate, Position vector
r_c	Vortex core radius
$R, \mathbf{R}$	Radius, Planet-centered radial coordinate
R_g	Specific gas constant

*Ph D. candidate, School of Aerospace Engineering, Georgia Institute of Technology, North Avenue, Atlanta, GA 30332

$\mathcal{R}$ Real part of a complex valued function
s Seconds
t Time
T Temperature
$\mathcal{T}$ Period of an orbit
u, v, w Components of velocity in the cartesian coordinates
$V, \mathbf{V}$ Velocity, Velocity vector
$\mathcal{V}$ Volume
x, y, z Body axis cartesian coordinate triad
$\tilde{x}, \tilde{y}, \tilde{z}$ Fluid element axis cartesian coordinate triad
α Angle of attack measured about the wind y-axis
β Angle of Yaw measured about the wind z-axis
γ Ratio of specific heats
Γ Vortex strength, Circulation
δ Boundary layer thickness
δ_{ij} Kronecker delta
ϵ A constant
ε Orbit or path eccentricity
ζ A constant
η A constant
θ Circumferential coordinate
Θ True anomaly/Perifocal circumferential coordinate
κ *Kwasu* function
λ Bulk viscosity
Λ Source/sink strength
μ Dynamic viscosity
μ_g Gravitational parameter
ν Kinematic viscosity
ξ Vorticity
Ξ Planetary longitude
ρ Density
ϱ Perifocal radial coordinate
σ A constant
τ Shear stress
φ, φ_i Azimuthal spherical coordinate, Orbit inclination
ϖ Angular velocity
Π Planetary Latitude
ϕ Classical velocity potential
Φ Gravitational potential
χ A constant
ψ, Ψ Classical stream function, Perifocal stream function
ω Vorticity vector
Ω Right ascension
Υ Argument of perigee

Subscript

0 Zero,Initial,Total or Stagnation condition
B Body
e Edge of boundary layer
p Planet
q Aerodynamic heat flux
R Rotated
s Separation point
Tr Transition point
w Conditions at the solid wall or surface
∞ Free stream

Operators

∇ Gradient operator
$\nabla\times$ Curl operator
$\nabla\cdot$ Divergence operator
∇^2 Laplacian operator
$\frac{D}{Dt}$ Substantial derivative

I. Introduction

Traditionally, the steady inviscid flow over a body can be obtained by solving the Euler equations with the appropriate boundary conditions or equivalently, by the superposition of elementary flows with known solutions[6]. This is in recognition of the fact that the velocity field of such a flow obeys the Laplace equation which is linear and lends itself to analytical solutions usually by the method of separation of variables. The theoretical simulation of the steady flow over a body in this manner results in a prediction of zero drag as opposed to the real case of some finite drag. This classical theoretical fluid dynamics problem[4] has persistently resisted an analytical solution despite much attention; a long standing paradox since 1768 when John Le Rond d'Alembert published his paper[6,12,28]. Classical inviscid theory falls short of reconciling the actions of fluid viscosity and frictional forces in a real flow with the theoretical analysis of such a flow. As such, it is unable to predict the very important phenomenon of flow separation which leads, in part, to the finite drag experienced by the body in a real flow. Nonetheless, the reign of the Laplace equation on inviscid flows has experimental evidences and its solutions for some bodies and configurations share some qualitative characteristics with real flows as exemplified by the streamlines of the unseparated flow over a circular cylinder or a sphere.

Real flows are viscous flows the physics of which are governed by the Navier-Stokes equations (NSE)[3,16,31]. Adequate solutions of the NSE would appropriately predict flow separation and result in some finite drag on a body within the flow. However, the NSE are highly complex and non-linear. Up to the point of writing, no known analytical solution of the full equations which gives the velocity and pressure fields of the flow as continuous functions of some specified freestream and boundary conditions with finite energy has been found for more than a century since the equations were formulated. In fact, at the turn of the 21st century, the Clay Mathematics Institute of Cambridge Massachussets (CMI) included finding a solution or the proof of a solution or the proof of no solutions to these equations as one of its seven millennium prize problems[31]. CMI has been at the forefront of the coordination of the worldwide search for the general solution(s) (or proof of no solution(s)) to these relations and a check on the status of the problem still reveals it to be unsolved despite some recent attempts by a number of researchers. However, with limiting but suitable assumptions and approximations, exact and approximate analytical solutions of these relations have been obtained for some special flows. Additionally, direct numerical solution of these relations over a discretized domain can be obtained with the use of high-speed computers. Depending on the complexity of the flow and the turbulence model used as well as the computational speed, such simulations can take days of computing.

Efforts at solving the NSE eventually led to the formulation of the Boundary layer theory (BLT) which simplifies the NSE into the boundary layer equations (BLE) in the early 1900s. In his proposition of the BLT, Prandtl recognised that the viscous effects in a wall bounded flow are largely confined to the thin boundary layer just adjacent to the wall. Prandtl's premise on the BLT is the experimentally backed assumption of the no-slip condition at the wall. He surmised that the no-slip condition, imposed on the flow by friction and the fluid viscosity, ensures that the fluid adheres to and also assumes the velocity of the wall. Since the velocity field of the flow is continuous,the fluid rapidly accelerates to the local freestream velocity at the edge of the boundary layer where inviscid theory holds reasonably. The boundary layer hypothesis has proven crucial in understanding and predicting viscous phenomena including flow separation and skin friction drag as well as aerodynamic heating. With Prandtl's submission, the solutions of the flow field around bodies have been obtained with inviscid theory applied outside the boundary layer coupled with the solution of the boundary layer equations. This has resulted in over a century of aerodynamic successes and has been generally considered as the resolution of the famed d'Alembert's paradox. Nonetheless, the no-slip boundary condition remains a largely controversial assumption[1,15] as exemplified by the recent work of Hoffman et al[19,27] who were able to compute drag with a slip boundary condition from the computational solution of the unsteady Euler equations with values comparable to those obtained in real experiments.

In stating the problem of the NSE as one of the prize problems, Fefferman emphasizes the physical realizability of any proposed solution as a major basis in assessing its acceptability[31]. This has to be so since the NSE are believed to adequately describe our understanding of the laws of nature applied to the flow of fluids. Particularly, he restricted the attention to the flow of an "*incompressible fluid*" possibly in an attempt to make the problem more tractable (the emphasis is added here to highlight that fluids are always compressible to a larger or smaller extent and this widely accepted and successful engineering assumption for some flows may detract from finding a closed form solution to the NSE which appropriately matches reality. This is also the view held by Muriel[32] who proposed an exact solution to the NSE in 2011 and noted that such density variations are pivotal to the propagation of sound waves in reality no matter how small the Mach number is). He proceeds to describe an acceptable solution as one which satisfies the unsteady incompressible continuity equation and the NSE with expressions for the velocity vector and pressure as continuous functions of time and three dimensional space. In addition, the energy of such solution(s) should be bounded over all times ($t \geq 0$) and space although some room is left to accommodate some spatial periodicity of the solution. Whilst the fluid can generally be under the action of some externally applied forces e.g. gravitational force, such forces are allowed to be taken identically equal to zero or be described by a potential function. Or as a proof of non-existence of a solution, an external force field is sought such that with a divergence-free initial velocity field, there exist no solutions for the pressure and the velocity field at later times[31].

Though not on the list of the prize problems, Fefferman notes that the search for unsteady analytic solution(s) of the three dimensional Euler equations is beset with similar difficulties and of equal importance to the understanding of fluid dynamics. In an era of advanced computing and sophisticated experimental methods, more than just being an academic pursuit, a successful solution will not only unravel the enduring d'Alembert's paradox but will advance the comprehension of fluid dynamic phenomena possibly including turbulence beyond what Fefferman notes as primitive[31]. Also, an analytic solution to these equations would be suitable in exploring the unbounded flow around bodies something of which can be challenging for real experiments as well as numerical ones[5]. Indeed, it may contribute to a dramatic decrease in the financial and time costs of the design processes of fluid dynamic vehicles and machines. It may very well help in the development of more robust computational fluid dynamics (CFD) codes for solving the flow over very complex geometries. Gautier et al opine that one of the daunting problems of code validation is the general non-existence of known exact solutions of the governing equations of fluid flow which in and by themselves are able to adequately describe phenomena as complex as flow separation,vortex dynamics and wake formation [and shocks] the resolutions of which are the much desired benchmarks of codes[5].

Fefferman reports that some of the already proposed solutions to these problems in two dimensions blow up in time and offer no directions to the behaviour of solutions in three dimensions. He makes no mention of whether an accepted solution would be that of a free flow or a wall-bounded flow and if wall-bounded, no indications as to the acceptable boundary condition at the wall leaving the leeway to researchers to work with what may be found most appropriate. He concludes noting that the problem outplays known standard mathematical methods for solving partial differential equations and calls for "deep,new ideas"[31].

The current author proposes '$\kappa(t, r, \theta, z, f, M_\infty, \gamma, \alpha, \beta, \mu_g)$ -*Kwasu* function'(KWASU is an acronym for Kwara State University in Malete, Nigeria where the idea was conceived by the current author and from which he gets funding for his ongoing graduate studies) as a solution to these equations by an extension of the results of classical inviscid theory of the flow over a circular cylinder.The flow over a circular cylinder has received attention from several theoretical and experimental investigators right from the earliest periods of fluid dynamics[11]. Even with its comparatively simple and basic geometry, its importance to fluid dynamic research resonates to the present in the study of Reynolds number effects on external wall-bounded bluff body flows and for the fact that it can lend itself to analytical investigations[12]. The physics of the real flow including separation, wake formation, vortex shedding, flow reattachment,compressibility effects e.t.c. are believed to be described by the NSE and were the benchmarks in the search for κ. With the premise that the classical inviscid theory holds, at least, at the front stagnation point and at the outer edge of the boundary layer, it is hypothesized that appropriate superposition of elementary flows with strengths determined from the results of the classical inviscid theory would yield a velocity field for the two dimensional incompressible flow over a circular cylinder which would satisfy the necessary conditions of a viscous wall-bounded flow via an intermediate stream function. The unsteady velocity field which is thus obtained is divergence-free identically and satisfies the no-slip condition in the steady-incompressible-flow-around-a-non-gravitating-body limit. In addition, important flow features such as flow separation,wake formation and the von-Kárman vortex street

are captured. The incompressible *Kwasu*-function is obtained by integrating the viscous stream function by rotation of the cartesian coordinate axes about the z-axis. This allows the integration of the pressure field out of the NSE. The density field is obtained using the definition of the isentropic speed of sound and the compressible Euler equations. From this, the compressible κ is obtained capturing compressibility effects in the flow field. With perfect gas assumption, the temperature field is obtained in turn. Equations yielding predictions of the points of transition to turbulent boundary layer flow and separation are derived. The solution will be mapped onto other geometries with some available analytical conformal mappings. An attempt will also be made to track the turbulence in the flow field by computing the change in entropy field in the entire flow domain in a future publication.

In section II, some review of literature is presented and the present theory is formulated in section III. The results are discussed in section IV. The paper ends with the concluding remarks in section V.

II. Background Studies and Review of Literature

The set of the NSE for the compressible flow of a fluid in an arbitrary control volume are expressed in single vector equations, using the indicial notation as

$$\oint\oint\oint_{\mathcal{V}} \left[\frac{\partial \rho}{\partial t} + \nabla \cdot (\rho \mathbf{V})\right] d\mathcal{V} = 0 \tag{1}$$

$$\oint\oint\oint_{\mathcal{V}} \left[\frac{D\,(\rho \mathbf{V})}{Dt} + \nabla p - \rho \mathbf{g} - \frac{\partial}{\partial x_j}\left[\mu\left(\frac{\partial v_i}{\partial x_j} + \frac{\partial v_j}{\partial x_i}\right) + \delta_{ij}\lambda \nabla^2 \mathbf{V}\right]\right] d\mathcal{V} = 0\ . \tag{2}$$

Equation 1 is a statement of the conservation of mass and Equation 2 embodies the conservation of momentum both of which arise from the application of those fundamental principles to the flow of fluids[16, 17, 31]. It is usually taken that the integrands in both equations are identically equal to zero at every point in the flow since the choice of the control volume here is arbitrary[16]. A number of different approaches to solving this problem exists based on the variables used. Either the solution is sought in terms of the primitive variables of velocity and pressure; or in terms of the stream function and vorticity; or in terms of the stream function alone[14].

In terms of the stream function and vorticity, the governing NSE for two dimensional constant property flow is presented in Equation 3 which is known as the vorticity equation and in which the choice of using the cylindrical polar coordinates is for convenience for the flow over the circular cylinder[2, 4, 9, 17, 18].

$$\begin{aligned} \xi &= -\left(\frac{1}{r}\frac{\partial}{\partial r}\left(r\frac{\partial \psi}{\partial r}\right) + \frac{1}{r^2}\frac{\partial^2 \psi}{\partial \theta^2}\right) \\ \frac{\partial \xi}{\partial t} + \frac{1}{r}\frac{\partial \psi}{\partial \theta}\frac{\partial \xi}{\partial r} - \frac{1}{r}\frac{\partial \psi}{\partial r}\frac{\partial \xi}{\partial \theta} &= \nu\left(\frac{1}{r}\frac{\partial}{\partial r}\left(r\frac{\partial \xi}{\partial r}\right) + \frac{1}{r^2}\frac{\partial^2 \xi}{\partial \theta^2}\right) \end{aligned} \tag{3}$$

Researchers have obtained numerical solutions of the two dimensional vorticity equation using available finite-differencing CFD methods. Some have also expanded the stream function and vorticity as truncated Fourier series, inserted them in Equation 3, and sought numerical solutions in what is clearly a semi-analytical method[9]. Results from such calculations form parts of a rich and extensive literature on the flow over a circular cylinder and have closely matched experimental trends sometimes more qualitatively than quantitatively. For $0 < f < 4$ (where the Reynolds number is based on the diameter of the cylinder), the creeping flow, the flow is almost steadily symmetrical about the longitudinal and lateral axes of the cylinder[10, 16]. A wake-like structure first becomes noticeable for f O(1)[10] and a stable pair of recirculating eddies forms in the wake after the flow separates aft of the cylinder for $f > 6$[10]. Generally, this recirculation region grows in length and width as a monotonic function of the Reynolds number[4, 22], however it is reported to diminish with increasing blockage ratio[22]. Additionally, some reported numerical results display a trend towards reduction of the streamwise extent of the bubble for some f between 10 and 100[22]. For $f > 40$, the recirculation region destabilizes, the flow becomes unsteady and asymmetric, and the vortices are shed periodically and alternately from the top and bottom sides of the cylinder to form the Von-Kárman vortex

street[10,16,17]. Accommodating this into a numerical computation of the flow have normally been achieved by artificially introducing a disturbance at some desired points of the flow and/or impulsively rotating the cylinder clockwise or counter-clockwise. Some investigators have been able to achieve such asymmetry in their numerical computations of the flow without any artificial means which Patel suggests was most likely due to truncation errors[10]. For larger f, the vortex street persists in forming a distinct wake. The laminar boundary layer separates from the forward face of the cylinder for sub-critical Reynolds numbers. At critical f, the separated flow region from the front face of the cylinder reattaches and later, separates aft of the cylinder. In the super-critical f regime, the boundary layer is fully turbulent and does not separate until aft of the cylinder[16]. While much is known and understood about the flow over the circular cylinder, there is still the unknown in the limit of infinite f where classical inviscid theory fails and no computational and/or experimental data exists.

The failure of steady inviscid theory in matching everyday experience in its prediction of the flow over a circular cylinder (or on any other body) is generally attributed to the loss of the no-slip condition at the cylinder surface believed to be imposed by the fluid viscosity. When the fluid is idealized as having no viscosity, it is generally the case that the only condition imposed at the surface is the impermeability condition on the normal velocity (for an impermeable wall) while the no-slip condition is rejected allowing some finite tangential fluid velocity at the surface[3]. Yet, the subject of the no-slip condition is a controversial one[1,3,15]. Even though it has been generally accepted as a universal empirical truth for viscous flows, compelling experimental and theoretical evidence have contested such claim of universality[1]. The occurrence of slip has been observed in gaseous flows in which the mean free path is large in comparison to the characteristic dimension of the walls of the container in which the gas is confined or that of a body over which the gas flows[1]. In a very recent paper, Brenner proposed a formula for the slip velocity which is a direct function of the gradient of the density at the surface[1]. Thus, he identified the fluid incompressibility as a necessary but *insufficient* condition for the application of the no-slip. The question then comes to mind, what would constitute a sufficient condition? On the microscopic level, the no-slip has been explained noting that the almost-omni-present surface roughness brings about the viscous dissipation of the fluid to rest regardless of the affinity between the fluid molecules and the solid surface[15]. Stokes, who was the pioneer proponent of the no-slip condition, justified it with various reasons, chief amongst which is the "highly satisfactory" agreement between experimental results and theoretical results which employ the condition[3]. A natural theoretical consequence of the acceptance of the no-slip condition is the proposition of the existence of the boundary layer by Prandtl[19]. The success of the ensuing boundary layer theory has since established the existence of a boundary layer has a signature of viscous wall bounded flows. This has been challenged only by a few[19]; Hoffman and Johnson reported a new resolution of d'Alembert's paradox by the numerical solution of the inviscid unsteady Euler equations employing a slip boundary condition at the surface throwing back the resolution of the famed paradox in the spotlight of controversy[19,28]. They argued that potential flow solutions are unstable to perturbations. Consequently, these develop into turbulent flow solutions which result into some finite drag on the body. They concluded, therefore, that drag results "mainly from the turbulent nature of the flow and only to a small part from viscous boundary layers"[19]. Indeed, in his appraisal of the no-slip condition, Day submitted that "the justification for using or not using the no-slip condition in model construction is based largely on "how successful the ultimate mathematical treatment will be""[3].

With a relatively very high velocity gradient at the wall, vorticity is introduced into the flow and convected downstream[12,16,19]. The vorticity effect of the boundary layer has been numerously idealized in theoretical solutions with an inviscid vortex sheet wrapping all around the body[12,16] as exemplified by the famous thin airfoil theory[16]. This is also the approach proposed by Helmholtz, and later Levi-Civita, in his contributions to the theoretical prediction of finite drag on a non-accelerating moving body in an inviscid fluid - the wake hypothesis[28]. Whilst been successful in the prediction of lift on the airfoil, it is less so with drag[16]. Traditionally, the non-lifting flow over bodies have been simulated with source/sink sheets and the lifting flow with vortex sheets in what is called the panel method. In order to overcome some problems encountered in the panel methods, some investigators have used the combination of sources, sinks and vortices in their panels[16]. In this work, such innovative ideas are employed idealizing the boundary layer flow as one consisting of contributions from local vortices and sources/sinks that are mutually concentric at every location on the wall.

III. Theoretical Formulation

A. Background

For a steady 'incompressible' flow, the velocity field is divergence-free and satisfies

$$\nabla \cdot \mathbf{V} = 0 \, .$$

Then ψ identically satisfies the divergence-free condition since

$$\mathbf{V} = \frac{1}{r}\frac{\partial \psi}{\partial \theta}\mathrm{e_r} - \frac{\partial \psi}{\partial r}\mathrm{e}_\theta + 0\mathrm{e_z}$$

and

$$\nabla \cdot \mathbf{V} = \frac{1}{r}\frac{\partial r V_r}{\partial r} + \frac{1}{r}\frac{\partial V_\theta}{\partial \theta} = \frac{1}{r}\frac{\partial^2 \psi}{\partial r \partial \theta} - \frac{1}{r}\frac{\partial^2 \psi}{\partial \theta \partial r} = 0 \, .$$

When the flow is considered irrotational in addition, then both ψ and ϕ satisfy the Laplace equation. Otherwise, ϕ is not defined, and ψ satisfies the continuity equation identically as well as the Poisson equation ($\nabla^2 \psi = -\omega_z = -\xi$) but not the Laplace equation. Separated variable solutions to the Laplace equation abound in mathematics literature. In a disc, the general solution is obtained as an infinite Fourier series for ψ and ϕ as

$$\begin{aligned} \psi(r,\theta) &= A_0 + B_0 \ln r + \sum_{m>0} \left(A_m r^m + B_m r^{-m}\right) \sin\left[m\left(\theta - \theta_m\right)\right] \\ \phi(r,\theta) &= A_0 - B_0 \theta + \sum_{m>0} \left(A_m r^m - B_m r^{-m}\right) \cos\left[m\left(\theta - \theta_0\right)\right] \, , \end{aligned} \tag{4}$$

where m is a positive integer and θ_m is an arbitrary constant angle. Depending on the values taking for m and the arbitrary constants in these equations, these solutions correspond to the inviscid lifting flow of a uniform free stream over a number of two dimensional geometries ranging from the circular cylinder ($m = 1$) to semi-infinite wedges ($m > 1$). These general solutions are identifiable as the superposition of elementary flows[29]. In this sense, the treatment and focus here on the circular cylinder using these solutions can be extended to the general case.

Equation 4 is rewritten as

$$\psi(r,\theta) = B_0 \ln\left(\frac{r}{R}\right) + \sum_{m>0} A_m r^m \sin\left[m\left(\theta - \theta_m\right)\right]\left(1 - \left(\frac{R_m^2}{r^2}\right)^m\right) \, , \tag{5}$$

in which $A_0 = -B_0 \ln R$ and $R_m^{2m} = -\frac{B_m}{A_m}$. To obtain the components of velocity, the stream function is differentiated in the relevant directions to give

$$V_r = \sum_{m>0} m A_m r^{m-1} \cos\left[m\left(\theta - \theta_m\right)\right]\left(1 - \left(\frac{R^2}{r^2}\right)^m\right) \, ,$$

$$V_\theta = -\frac{B_0}{r} - \sum_{m>0} m A_m r^{m-1} \sin\left[m\left(\theta - \theta_m\right)\right]\left(1 + \left(\frac{R^2}{r^2}\right)^m\right)$$

and

$$V = \sqrt{\left(\sum_{m>0} m A_m r^{m-1} \cos\left[m\left(\theta - \theta_m\right)\right]\left(1 - \left(\frac{R^2}{r^2}\right)^m\right)\right)^2 + \left(-\frac{B_0}{r} - \sum_{m>0} m A_m r^{m-1} \sin\left[m\left(\theta - \theta_m\right)\right]\left(1 + \left(\frac{R^2}{r^2}\right)^m\right)\right)^2} \, .$$

(6)

For the non-lifting flow (NLF) over a circular cylinder in which the uniform flow is parallel to the x-axis, $B_0 = \theta_m = 0, m = 1, A_1 = V_\infty$, $B_1 = \frac{k}{2\pi}$ and $R^2 \equiv \frac{k}{2\pi V_\infty}$ in Equation 5 and the corresponding expressions for its velocity field[16]. The free stream is assumed to be steady and uniform. However, in an unsteady flow and for a flow in the vicinity of a planet, the acceleration of the center of mass of the moving body needs to be taken into account. Therefore, a general form of the free stream velocity is presented in Equation 7 which describes the relative motion of a body around a planet rotating with a constant angular velocity[35]. The inclusion of this 'planetary effect'(more widely known as the Coriolis effect) in this formulation is justified with the observations and conclusions of Shapiro[36] that the rotation of the Earth as well as the geographical location of an observer have some subtle effect on the direction of swirl of a bath-tub vortex. In addition, the wake shed from a body flying in the Earth's atmosphere descends partly under the influence of gravity[37]. It is also in agreement with Newton's observations on and law of universal gravitation which are suggestive that much may be lost were gravitational effects allowed to be buried in the foregoing study under the frequent assumption/simplification of 'no body forces'. Fortunately, the gravitational force field is a conservative field which can be described by a potential function governed by the linear Laplace equation in three dimensions[30,35].

$$\mathbf{V}_0 = \left[\dot{x} + \varpi\left(R_p + z\right)\cos\Pi\right]\hat{\mathbf{i}} + \dot{y}\hat{\mathbf{j}} + \dot{z}\hat{\mathbf{k}}$$

$$\mathbf{a}_\infty = \left[\ddot{x} + \frac{\dot{x}\left(\dot{z} - \dot{y}\tan\Pi\right)}{R_p + z} + 2\varpi\left(\dot{z}\cos\Pi - \dot{y}\sin\Pi\right)\right]\hat{\mathbf{i}} + \left[\ddot{y} + \frac{\dot{y}\dot{z} + \dot{x}^2\tan\Pi}{R_p + z} + \varpi\sin\Pi\left[\varpi\left(R_p + z\right)\cos\Pi + 2\dot{x}\right]\right]\hat{\mathbf{j}}$$

$$+ \left[\ddot{z} - \frac{\dot{x}^2 + \dot{y}^2}{R_p + z} - \varpi\cos\Pi\left[\varpi\left(R_p + z\right)\cos\Pi + 2\dot{x}\right]\right]\hat{\mathbf{k}}$$

$$\mathbf{V}_\infty = \mathbf{V}_0 + \int \mathbf{a}_\infty dt$$

(7)

In addition, the complex gravitational interactions between the body(ies) in motion, the fluid medium and the planet(s) can be modeled as linear combinations of 'two-body problems' each described by the gravitational potential presented in Equation 8 which is obtained by separated variables solution of the Laplace equation in the spherical polar coordinate system[30,34] and in which $\mu_g = G\mathcal{M}_p$ and $\mathbf{R} = R_p + H + z$. The form of this solution of the Laplace equation presented here as reported by Pines[34] is optimized to remove singularities at the zonal poles.

$$\Phi(\mathbf{R}, \Xi, \Pi) = \frac{\mu_g}{\mathbf{R}}\left[1 + \sum_{n=1}^{\infty}\left(\frac{R_B}{\mathbf{R}}\right)^n \sum_{m=1}^{n}\frac{1}{2^n n!}\frac{d^{n+m}}{d(\sin\Pi)^{n+m}}\left(\sin^2\Pi - 1\right)^n\left(C_{n,m}\left(\cos m\Xi\cos m\Pi\right) + S_{n,m}\left(\sin m\Xi\cos m\Pi\right)\right)\right]$$

(8)

In Equation 8, $C_{n,m}$ and $S_{n,m}$ are unique mass coefficients that are obtained from observations of satellite motions about a planet[35] and may be inferred from controlled experiments in the case of a vehicle for instance.

With the appropriate choice for the constants and the integer in Equation 4, the stream function for a potential sink/source, and the radial velocity can be expressed as

$$\psi = \frac{\Lambda}{2\pi}\theta$$
$$V_r = \frac{\Lambda}{2\pi r}\ .$$

(9)

Similarly, the potential solution for a vortex can be obtained as

$$\psi = \frac{\Gamma}{2\pi}\ln r$$

$$V_\theta = -\frac{\Gamma}{2\pi r} \ . \tag{10}$$

However, Equation 3 can be specialized for a line viscous vortex giving rise to the heat equation for which various analytic solutions also exist in the literature[18]. Amongst such solutions is the Lamb-Oseen vortex model.The circulation for this model is given as

$$\Gamma = \int_0^r 2\pi r \xi dr = -\Gamma_0 \left[exp^{\left(-\frac{r^2}{r_c^2}\right)} \right]_0^r , \tag{11}$$

where Γ_0 is the initial circulation and $r_c^2 = 4\nu t$. This is a time-dependent model of the viscous diffusion of a line vortex. When the time component in the equation is fixed, this vortex solution becomes the Burgers vortex model. Burgers vortices have been used to model eddies in turbulent flows successfully[18].

B. Main Hypothesis

To simulate the boundary layer effect theoretically in the NLF, the cylindrical surface is replaced with a viscous sink-source-vortex sheet which has the sinks/sources and the vortices positioned at the same locations. The strengths of the sinks/sources and vortices are dictated by the velocity field of the NLF.Additionally, their locations are dictated by the dividing streamline equation for the NLF. Also, the strengths of a sink /source and vortex at a specific location are not the same but vary in a manner that reflects the actual physics of the real flow with one varying with the sine of the angular location and the other with the cosine.

C. Model

The model is started by assuming the vortices generated by the imposition of the no-slip condition at the cylinder wall can be represented as Burgers vortices. The circulation introduced by these vortices is then represented as

$$\Gamma = \Gamma_0 exp^{\left(-\frac{(r-R)^2}{r_c^2}\right)} \tag{12}$$

where the radial distance, r, in Equation 11 has been replaced with $r - R$ and the bounds of the integration are discarded. An analytic expression for the initial circulation is obtained from the NLF

$$V_\theta = -V_\infty \sin\theta \left(1 + \frac{R^2}{r^2}\right) = \frac{\Gamma_0}{2\pi r} \ ,$$

so that the initial circulation of the surface vortices is

$$\Gamma_0 = -2\pi V_\infty \sin\theta r \left(1 + \frac{R^2}{r^2}\right)$$
$$\pi \geq \theta \geq \ -\pi \ . \tag{13}$$

The 'characteristic time', t of the vortices at any specific location which is required to express the vortex core radius analytically is modeled as the distance from the cylindrical surface to that location divided by the 'speed' at the location obtained from the NLF altogether multiplied by some f-dependent spatial and temporal constant. Therefore

$$t = \frac{f_\infty^2}{130\,(0.03061 f_\infty)^{\mathrm{e}^{\frac{10}{f_\infty}}}} \frac{(r-R)}{V_\infty \sqrt{\left(1-\frac{R^2}{r^2}\right)^2 + 4\,\frac{R^2 \sin^2\theta}{r^2}} + 2}\ , \tag{14}$$

giving

$$r_c^2 = \frac{f_\infty^2}{130\,(0.03061 f_\infty)^{\mathrm{e}^{\frac{10}{f_\infty}}}} \frac{4\nu_\infty\,(r-R)}{V_\infty \sqrt{\left(1-\frac{R^2}{r^2}\right)^2 + 4\,\frac{R^2 \sin^2\theta}{r^2}} + 2}\ . \tag{15}$$

The number '2' added to the expression for the NFL speed is needed to remove discontinuities in the expression when $r = R$ and $\theta = \pm\pi, 0$. Now, Equation 15 is employed in Equation 12 to obtain the Reynolds-number-dependent strength of the surface vortex sheet as

$$\Gamma = -2\,\pi V_\infty\, r \sin\theta \left(1+\frac{R^2}{r^2}\right) \mathrm{e}^{-\left(\frac{r^2}{V_\infty^2 t^2} + \frac{130(0.03061 f_\infty)^{\mathrm{e}^{\frac{10}{f_\infty}}}}{8 f_\infty} \sqrt{\left(1-\frac{R^2}{r^2}\right)^2 + 4\,\frac{R^2\sin^2\theta}{r^2}} + 2\left(\frac{r}{R}-1\right)\right)}\ , \tag{16}$$

where the term in t in the exponent has been added to model the temporal evolution of the surface vortex strength starting from an initial value of zero at $t = 0$. The addition of this term changes the model of the surface vortices to a hybrid Lamb-Oseen-Burgers vortex.

The definition of the stream functions in Equations 9 and 10 is arbitrary, that is, values need to be chosen for A_0 in Equation 4 from which they can be obtained. Thus, constants $-\frac{\Gamma}{2\pi}\ln R$ and $\frac{\Lambda}{2\pi}\sigma$ are introduced as follows

$$\psi_{vortex} = \frac{\Gamma}{2\pi}\ln r - \frac{\Gamma}{2\pi}\ln R = \frac{\Gamma}{2\pi}\ln\frac{r}{R}$$

$$\psi_{source/sink} = \frac{\Lambda}{2\pi}\left(\theta+\sigma\right)\ ,$$

where σ takes on the values of $\pm\pi$ depending on the semicircle of the cylinder. The introduction of these constants helps in (1)enforcing the no-slip condition at the wall in the case of $\ln\frac{r}{R}$ and (2) making sure that the stagnation point is appropriately placed in front of the cylinder in the case of σ. In addition, $-\frac{\Gamma}{2\pi}\ln R$ can be understood as the natural reaction (based on Newton's third law) at the wall to the introduction of a vortex into the flow i.e. the surface vortex in the foregoing context. Hence, the stream function for the vortex sheet is given as

$$\psi_{vortex} = -V_\infty r \sin\theta \left(1+\frac{R^2}{r^2}\right) \ln\left(\frac{r}{R}\right) \mathrm{e}^{-\left(\frac{r^2}{V_\infty^2 t^2} + \frac{130(0.03061 f_\infty)^{\mathrm{e}^{\frac{10}{f_\infty}}}}{8 f_\infty} \sqrt{\left(1-\frac{R^2}{r^2}\right)^2 + 4\,\frac{R^2\sin^2\theta}{r^2}} + 2\left(\frac{r}{R}-1\right)\right)}\ . \tag{17}$$

If the singularities (vortices and sources/sinks) generated at the surface in a real flow are actually concentric as hypothesized, then the radial velocity obtained from the vortex sheet will be equal to that expected from the source/sink sheet. Therefore, to set the strength of the source/sink on the cylindrical surface, Equation 9 is employed noting that the radial velocity is obtained from Equation 17 as

$$V_r = -V_\infty \left(1+\frac{R^2}{r^2}\right) \ln\left(\frac{r}{R}\right) \left(\cos\theta - \frac{65\,(0.03061 f_\infty)^{\mathrm{e}^{\frac{10}{f_\infty}}}}{f_\infty} \frac{\sin^2\theta\cos\theta\left(\frac{r}{R}-1\right)\frac{R^2}{r^2}}{\sqrt{\left(1-\frac{R^2}{r^2}\right)^2 + 4\,\frac{R^2\sin^2\theta}{r^2}} + 2}\right)$$

$$\mathrm{e}^{-\left(\frac{r^2}{V_\infty^2 t^2}+\frac{130(0.03061 f_\infty)^{\mathrm{e}^{\frac{10}{f_\infty}}}}{8 f_\infty}\sqrt{\left(1-\frac{R^2}{r^2}\right)^2+4\,\frac{R^2\sin^2\theta}{r^2}}+2\left(\frac{r}{R}-1\right)\right)},$$

so that the strength of the surface sink/source is

$$\Lambda = -2\pi V_\infty r\left(1+\frac{R^2}{r^2}\right)\ln\left(\frac{r}{R}\right)\left(\cos\theta-\frac{65\,(0.03061 f_\infty)^{\mathrm{e}^{\frac{10}{f_\infty}}}}{f_\infty}\,\frac{\sin^2\theta\cos\theta\left(\frac{r}{R}-1\right)\frac{R^2}{r^2}}{\sqrt{\left(1-\frac{R^2}{r^2}\right)^2+4\,\frac{R^2\sin^2\theta}{r^2}+2}}\right)$$

$$\mathrm{e}^{-\left(\frac{r^2}{V_\infty^2 t^2}+\frac{130(0.03061 f_\infty)^{\mathrm{e}^{\frac{10}{f_\infty}}}}{8 f_\infty}\sqrt{\left(1-\frac{R^2}{r^2}\right)^2+4\,\frac{R^2\sin^2\theta}{r^2}}+2\left(\frac{r}{R}-1\right)\right)}.$$

The strength varies largely with the cosine of the angle and the remnant of the initial NFL has been carried over in the $\left(1+\frac{R^2}{r^2}\right)$ term. The source/sink sheet strength can be viewed as having a contribution from the uniform flow and another from the doublet. However, these two components should have alternate senses. Examination of the real flow over the cylinder dictates the senses of the sinks/sources. At the front stagnation point for instance, where $\cos\theta$ is negative, the reverberation of the fluid momentum back into the upstream flow suggests that such reverberation must be treated as if coming from a local source on the base doublet at that point. Thus, it is more physically appropriate to employ the equation

$$\Lambda = 2\pi V_\infty r\left(1-\frac{R^2}{r^2}\right)\ln\left(\frac{r}{R}\right)\left(\cos\theta-\frac{65\,(0.03061 f_\infty)^{\mathrm{e}^{\frac{10}{f_\infty}}}}{f_\infty}\,\frac{\sin^2\theta\cos\theta\left(\frac{r}{R}-1\right)\frac{R^2}{r^2}}{\sqrt{\left(1-\frac{R^2}{r^2}\right)^2+4\,\frac{R^2\sin^2\theta}{r^2}+2}}\right)$$

$$\mathrm{e}^{-\left(\frac{r^2}{V_\infty^2 t^2}+\frac{130(0.03061 f_\infty)^{\mathrm{e}^{\frac{10}{f_\infty}}}}{8 f_\infty}\sqrt{\left(1-\frac{R^2}{r^2}\right)^2+4\,\frac{R^2\sin^2\theta}{r^2}}+2\left(\frac{r}{R}-1\right)\right)}, \tag{18}$$

in which $\left(1+\frac{R^2}{r^2}\right)$ has been replaced by $\left(1-\frac{R^2}{r^2}\right)$ and the leading negative sign dropped. Hence, the Reynolds-number-dependent stream function of the source/sink sheet is given by

$$\psi_{sink/source} = V_\infty r\left(1-\frac{R^2}{r^2}\right)\ln\left(\frac{r}{R}\right)\left(\cos\theta-\frac{65\,(0.03061 f_\infty)^{\mathrm{e}^{\frac{10}{f_\infty}}}}{f_\infty}\,\frac{\sin^2\theta\cos\theta\left(\frac{r}{R}-1\right)\frac{R^2}{r^2}}{\sqrt{\left(1-\frac{R^2}{r^2}\right)^2+4\,\frac{R^2\sin^2\theta}{r^2}+2}}\right)(\theta+\sigma)$$

$$\mathrm{e}^{-\left(\frac{r^2}{V_\infty^2 t^2}+\frac{130(0.03061 f_\infty)^{\mathrm{e}^{\frac{10}{f_\infty}}}}{8 f_\infty}\sqrt{\left(1-\frac{R^2}{r^2}\right)^2+4\,\frac{R^2\sin^2\theta}{r^2}}+2\left(\frac{r}{R}-1\right)\right)}. \tag{19}$$

Equation 19 is needed to ensure that the tangential velocity does not vanish above the surface of the cylinder when $\theta = 0$ in agreement with the real flow and away from the classical theoretical prediction from Equation 5. However, when employed in this manner, it gives rise to a non-vanishing surface vorticity at $\theta = 0$ which is also non-physical. Therefore, Equation 19 is modified into

$$\psi_{sink/source} = V_\infty r\left(1-\frac{R^2}{r^2}\right)\ln\left(\frac{r}{R}\right)\left(\cos\theta-\frac{65\,(0.03061 f_\infty)^{\mathrm{e}^{\frac{10}{f_\infty}}}}{f_\infty}\,\frac{\sin^2\theta\cos\theta\left(\frac{r}{R}-1\right)\frac{R^2}{r^2}}{\sqrt{\left(1-\frac{R^2}{r^2}\right)^2+4\,\frac{R^2\sin^2\theta}{r^2}+2}}\right)$$

$$((\theta+\sigma)\,\chi\sin(\theta+\epsilon))^{\mathrm{e}^{-\frac{\mathrm{a}_\infty \mathrm{t}}{\mathrm{r}}\left(1-\frac{\mathrm{R}}{\mathrm{r}}\right)}}\ \mathrm{e}^{-\left(\frac{r^2}{V_\infty^2 t^2}+\frac{130(0.03061 f_\infty)^{\mathrm{e}^{\frac{10}{\mathrm{f}_\infty}}}}{8 f_\infty}\sqrt{\left(1-\frac{R^2}{r^2}\right)^2+4\,\frac{R^2\sin^2\theta}{r^2}}+2\left(\frac{r}{R}-1\right)\right)},$$

$$\epsilon=\begin{cases}0.001\ , & \theta\geq 0\\ -0.001, & \theta<0\end{cases}$$

$$\sigma=\begin{cases}-(\pi+\epsilon)\,, & \theta\geq 0\\ \pi-\epsilon, & \theta<0\end{cases}$$

$$\chi=\begin{cases}1\ , & \theta\geq 0\\ -1\ , & \theta<0\end{cases}$$

(20)

in which $((\theta+\sigma)\,\chi\sin(\theta+\epsilon))^{\mathrm{e}^{-\frac{\mathrm{a}_\infty \mathrm{t}}{\mathrm{r}}\left(1-\frac{\mathrm{R}}{\mathrm{r}}\right)}}$ has been used to multiply Equation 19 to enforce the vanishing of the vorticity at $\theta=0$ for $r=R$ at the wall and at $r=\infty$ allowing for spatial variation between these boundaries with the term depending on the freestream speed of sound. ϵ is incorporated into this equation to remove singularities at $\theta=0,\pm\pi$ and χ sets the symmetry of the flow as $\pi\geq\theta\geq-\pi$. The gravitational field of a body (the cylinder in the present case) is given as

$$\Phi(r,\theta,\varphi)=\frac{\mu_g}{r}\left[1+\sum_{n=1}^{\infty}\left(\frac{R_B}{r}\right)^n\sum_{m=1}^{n}\frac{1}{2^n n!}\frac{d^{n+m}}{d(\sin\varphi)^{n+m}}\left(\sin^2\varphi-1\right)^n\left(C_{n,m}\left(\cos m\theta\cos m\varphi\right)+S_{n,m}\left(\sin m\theta\cos m\varphi\right)\right)\right],$$

(21)

where $\mu_g=G\mathcal{M}_B$. As mentioned before, $C_{n,m}$ and $S_{n,m}$ are unique mass coefficients which will have to be determined empirically. However, Fitzpatrick[30] presents

$$\Phi(r)=-\frac{\mu_g}{r}\left[1+\frac{1}{4}\left(\frac{R_B}{r}\right)^2+\frac{9}{64}\left(\frac{R_B}{r}\right)^4+\ldots\right]$$

(22)

for the potential due to a uniform ring centered on the origin lying in the x-y plane. This is employed as a suitable approximation for the cylinder in the present work. Since the differentials of the gravitational potential give the components of gravitational acceleration, the gravitational velocity potential is derived by integrating the gravitational potential in the perifocal temporal frame (t_ϱ). The possible transient variation of the gravitating body(ies) have to be taken into account in obtaining this integral. For a steady and uniform mass distribution in the cylinder, the gravitational velocity potential is thus obtained as

$$\phi(r,t_\varrho)=\int\Phi(r)\,dt_\varrho+\phi(r)$$
$$=-\frac{\mu_g(t_\varrho-\mathcal{T})}{r}\left[1+\frac{1}{4}\left(\frac{R_B}{r}\right)^2+\frac{9}{64}\left(\frac{R_B}{r}\right)^4+\ldots\right].$$

(23)

In this equation, the constant of integration which is dependent on r is conveniently chosen to be also a function of the period of the fluid element in 'orbit' around the cylinder so that the time in this perifocal frame varies periodically from 0 to $\mathcal{T}$.

The path(s) of two bodies moving solely under the influence of mutual gravity is(are) Keplarian orbits (conic sections) defined by

$$\varrho=\frac{h^2}{\mu_g}\frac{1}{1+\varepsilon\cos\Theta}$$

(24)

with the origin coinciding with the center of mass of the two-body system located at one of the foci of the orbit[30,35]. In the case of a fluid particle and the cylinder considered here, this origin is essentially located at the center of mass of the cylinder. In this perifocal frame of reference for the fluid particle motion under mutual gravitational influence with the body, the particle's velocity components are defined as

$$\begin{aligned} V_\Theta &= \frac{\mu_g}{h}\left(1+\epsilon\cos\Theta\right) = -\frac{\partial\Psi}{\partial\varrho} \\ V_\varrho &= \frac{\mu_g}{h}\epsilon\sin\Theta = \frac{1}{\varrho}\frac{\partial\Psi}{\partial\Theta}\ . \end{aligned} \tag{25}$$

In Equation 25, an indication of the existence of a perifocal stream function satisfying the 'steady' continuity equation identically in the perifocal frame of reference is included. This perifocal stream function is integrated out to be

$$\Psi = -\frac{\mu_g\varrho}{h}(1+\epsilon\cos\Theta)\ . \tag{26}$$

With further indications that the Keplerian orbit eccentricity is

$$\varepsilon = \sqrt{1+\frac{h^2}{\mu_g^2}(V^2-\frac{2\mu_g}{\varrho})} \tag{27}$$

and the true anomaly is

$$\Theta = \cos^{-1}\left[\frac{1}{\varepsilon}\left(\frac{h^2}{\mu_g\varrho}-1\right)\right]\ , \tag{28}$$

the expression for the perifocal stream function is found to simplify to

$$\Psi = -h\ . \tag{29}$$

Since the origins of the body axis and the perifocal frame are coincident, r and ϱ are similar and/or linearly dependent. This allows for the calculation of the specific angular momentum of the fluid particle in the 'orbit' around the cylinder in the body axis as

$$\begin{aligned} \mathbf{h} &= \mathbf{r}\times\mathbf{V} \\ h &= r\sqrt{V_\theta^2+V_z^2}\ . \end{aligned} \tag{30}$$

Differentiating Equation 23 appropriately gives the gravitational velocity components around the cylinder as

$$\begin{aligned} V_\theta &= 0 \\ V_z = \frac{\partial\phi}{\partial r}\frac{\partial r}{\partial z} &= -\frac{\mu_g(t_\varrho-\mathcal{T})\cos\left(\varphi-\frac{\pi}{2}\right)}{r^2}\left[1+\frac{1}{4}\left(\frac{R_B}{r}\right)^2+\frac{9}{64}\left(\frac{R_B}{r}\right)^4+\ldots\right]\ . \end{aligned} \tag{31}$$

Hence,

$$\begin{aligned} \psi_{gravity} &= \Psi = -h \\ &= \frac{\mu_g(t_\varrho-\mathcal{T})\cos\left(\varphi-\frac{\pi}{2}\right)}{r}\left[1+\frac{3}{4}\left(\frac{R_B}{r}\right)^2+\frac{45}{64}\left(\frac{R_B}{r}\right)^4+\ldots\right]\ . \end{aligned} \tag{32}$$

The orbital period is given as

$$\mathcal{T} = \frac{2\pi}{\mu_g^2}\left(\frac{h}{\sqrt{1-\varepsilon^2}}\right)^3 . \tag{33}$$

Therefore, the stream function of the uniform flow on a circular cylinder with the viscous boundary layer effect simulated by a viscous source-sink-vortex sheet is given by

$$\begin{aligned}
\psi &= \psi_{NLF} + \psi_{vortex} + \psi_{sink/source} + \psi_{gravity} \\
&= V_\infty r\sin\theta\left(1-\frac{R^2}{r^2}\right) - V_\infty r\sin\theta\left(1+\frac{R^2}{r^2}\right)\ln\left(\frac{r}{R}\right)\mathrm{e}^{-\left(\frac{r^2}{V_\infty^2 t^2}+\frac{130(0.03061 f_\infty)^{\mathrm{e}^{\frac{10}{f_\infty}}}}{8 f_\infty}\sqrt{\left(1-\frac{R^2}{r^2}\right)^2+4\,\frac{R^2\sin^2\theta}{r^2}}+2\left(\frac{r}{R}-1\right)\right)} \\
&\quad + V_\infty r\left(1-\frac{R^2}{r^2}\right)\ln\left(\frac{r}{R}\right)\left(\cos\theta - \frac{65\left(0.03061 f_\infty\right)^{\mathrm{e}^{\frac{10}{f_\infty}}}}{f_\infty}\,\frac{\sin^2\theta\cos\theta\left(\frac{r}{R}-1\right)\frac{R^2}{r^2}}{\sqrt{\left(1-\frac{R^2}{r^2}\right)^2+4\,\frac{R^2\sin^2\theta}{r^2}+2}}\right) \\
&\quad ((\theta+\sigma)\,\chi\sin(\theta+\epsilon))^{\mathrm{e}^{-\frac{\mathrm{a}_\infty \mathrm{t}}{\mathrm{r}}\left(1-\frac{\mathrm{R}}{\mathrm{r}}\right)}}\,\mathrm{e}^{-\left(\frac{r^2}{V_\infty^2 t^2}+\frac{130(0.03061 f_\infty)^{\mathrm{e}^{\frac{10}{f_\infty}}}}{8 f_\infty}\sqrt{\left(1-\frac{R^2}{r^2}\right)^2+4\,\frac{R^2\sin^2\theta}{r^2}}+2\left(\frac{r}{R}-1\right)\right)} \\
&\quad + \frac{\mu_g(t_\varrho-\mathcal{T})\cos\left(\varphi-\frac{\pi}{2}\right)}{r}\left[1+\frac{3}{4}\left(\frac{R_B}{r}\right)^2+\frac{45}{64}\left(\frac{R_B}{r}\right)^4+\ldots\right].
\end{aligned}$$

$$\epsilon = \begin{cases} 0.001\ , & \theta \geq 0 \\ -0.001, & \theta < 0 \end{cases}$$

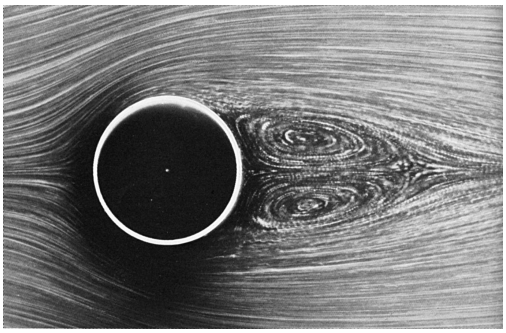
$$\sigma = \begin{cases} -(\pi+\epsilon)\,, & \theta \geq 0 \\ \pi-\epsilon, & \theta < 0 \end{cases}$$

$$\chi = \begin{cases} 1\ , & \theta \geq 0 \\ -1\ , & \theta < 0 \end{cases}$$

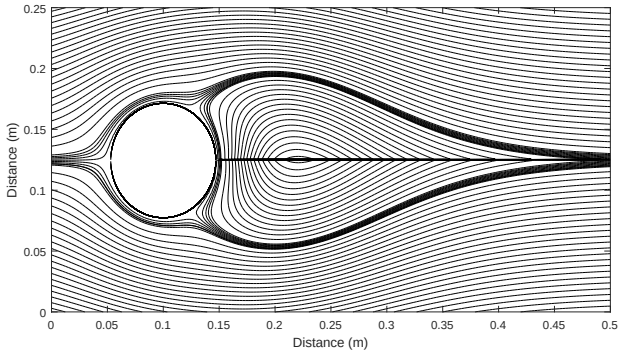
(34)

IV. Results and Discussion

One of the advantages of using the stream function formulation for finding solutions to the NSE is that the streamlines can directly be plotted from such solutions and compared immediately with those of the real flow. Such comparison is presented in Figure 1.



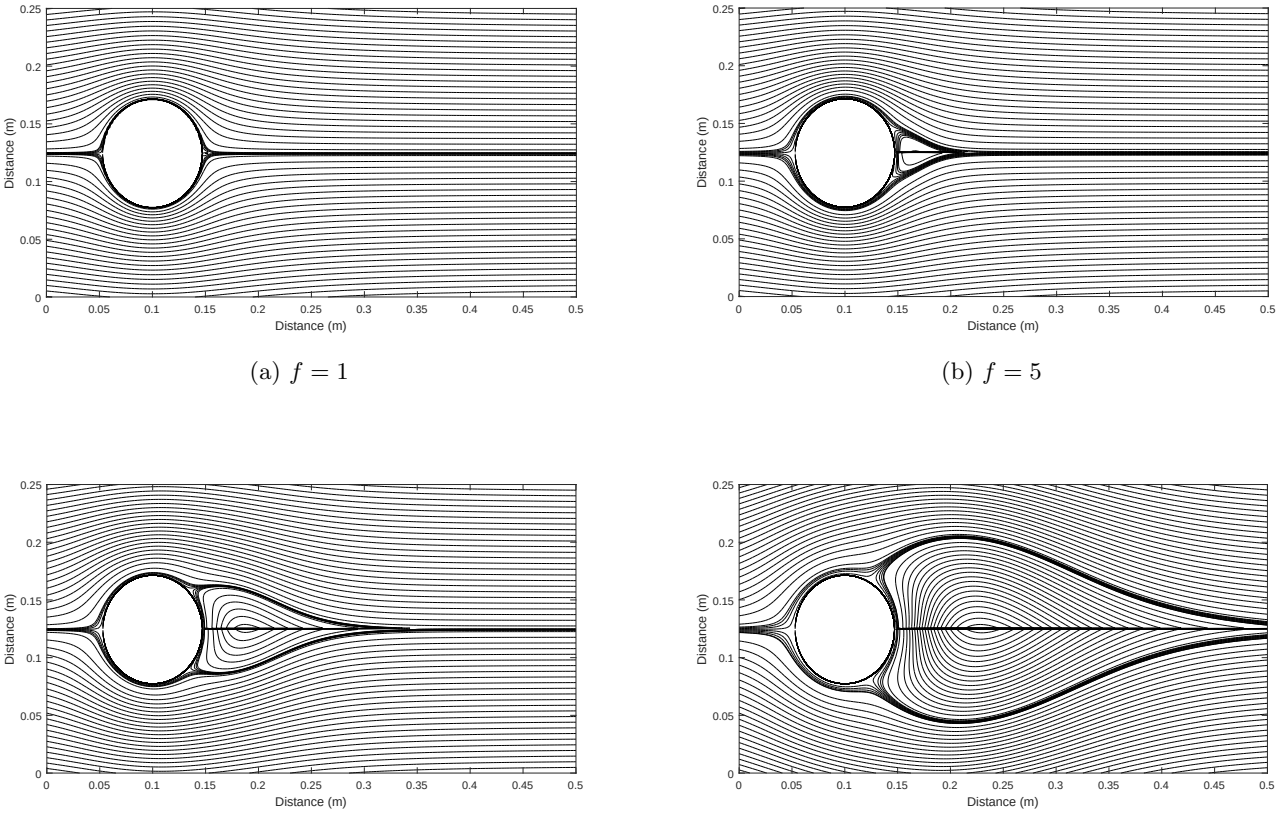
(a) The real flow over a circular cylinder[16].



(b) The streamlines predicted using Equation 34 for $\mathcal{M}_B = 1kg$ and $G = 6.67408 \times 10^{-11} m^3 kg^{-1} s^{-2}$.

Figure 1: Comparison between streamlines of the real flow and the present theoretical flow over the Cylinder at $f = 26$

In this figure and all subsequent figures showing streamlines, the flow is from left to right. The qualitative similarity is observable. However, the 'eyes' of the stationary wake vortices are very much closer to the centerline in the theoretical result than they are in the real flow. In agreement with what exists in the literature regarding the progressive growth of the wake dimensions with f[4, 22], Figure 2 presents such a trend as captured by Equation 34.



(a) $f = 1$ (b) $f = 5$

(c) $f = 10$ (d) $f = 40$

Figure 2: Comparison of the present theoretical predictions of the streamlines for $f = 1, 5, 10, 40$ and $\mathcal{M}_B = 1kg$. Observe how the wake enlarges with progressive f.

Examining the third term of Equation 34, it is evident that there may be a bias with θ if the conventional way in which θ varies from $0 - 2\pi$ is assumed. It is in a bid to avoid this that θ is taken to vary from 0 at the rear stagnation point to $+\pi$ at the front stagnation point on the upper half of the cylinder; and from 0 at the rear stagnation point to $-\pi$ at the front stagnation point for the lower half. As noted earlier, it is important to set σ appropriately as defined in the equation to ensure that the flow stagnates at the front stagnation point where $\theta = \pm\pi$ and no where else. The conditions on the stream function are to satisfy the continuity equation as well as the dual boundary conditions at infinity and at the surface. Verifying these would be algebraically laborious without the use of a mathematical software like *Maple*. It was confirmed that

$$\frac{1}{r}\frac{\partial}{\partial r}(rV_{r}) + \frac{1}{r}\frac{\partial}{\partial \theta}(V_{\theta}) = 0 \ .$$

As f increases to about 50, the real flow around the circular cylinder undergoes a Hopf bifurcation and the stationary counter-rotating vortices begin to shed into the von-Kárman vortex street. Theoretical simulations of this process are rare particularly when the street is shed from a bluff body. Föppl attempted to theorize the stable separated flow before the bifurcation by placing two vortices behind the cylinder. However, the ensuing surface pressure distribution was unphysical[20]. Others have also treated the vortex street as staggered double row point vortices or used vortex patch arrays[18]. In the present study, it was recognized that the exponential form of Equation 20 which was identified to produce the bubble in the flow can be exploited to model this interesting physical phenomenon by forming a product of some of the exponential argument with an appropriate function in the complex plane. Thus, Equation 20 was modified

into

$$\psi_{vortexshedding} =$$

$$\frac{V_\infty}{\zeta} r\left(1-\frac{R^2}{r^2}\right)\ln\left(\frac{r}{R}\right)\left(\cos\theta - \frac{65\left(0.03061 f_\infty\right)^{\mathrm{e}^{\frac{10}{f_\infty}}}}{f_\infty}\frac{\sin^2\theta\cos\theta\left(\frac{r}{R}-1\right)\frac{R^2}{r^2}}{\sqrt{\left(1-\frac{R^2}{r^2}\right)^2+4\frac{R^2\sin^2\theta}{r^2}+2}}\right)\left(\left(\theta+\sigma\right)\chi\sin\left(\theta+\epsilon\right)\right)^{\mathrm{e}^{-\frac{a_\infty t}{r}\left(1-\frac{R}{r}\right)}}$$

$$\mathrm{e}^{-\left(\frac{125}{f_\infty}+\frac{r^2}{V_\infty^2 t^2}\right)-\left(\mathrm{e}^{-\frac{130}{f_\infty}\left(\frac{r}{\sqrt{R^2+4\nu t}}-1\right)^2+\frac{130\left(0.03061 f_\infty\right)^{\mathrm{e}^{\frac{10}{f_\infty}}}}{8 f_\infty}\sqrt{\left(1-\frac{R^2}{r^2}\right)^2+4\frac{R^2\sin^2\theta}{r^2}+2}\left(\frac{r(t)}{R}-1\right)}\right)\left(\sin^2(\theta)+(\eta)^{\frac{-\frac{r^2}{4V_\infty^2 t^2}}{2}}\right)}, \tag{35}$$

in which

$$r(t) = r\sqrt{\left(\sin\theta - \frac{V_\infty t}{r}\left(\frac{R^2}{r^2}\sin\theta\cos\theta\right)\right)^2 + \left(\cos\theta - \frac{V_\infty t}{r}\left(1+\frac{R^2}{r^2}\left(\sin^2\theta-\cos^2\theta\right)\right)\right)^2}, \tag{36}$$

$$\eta = \begin{cases} 1\ , & \theta > \frac{\pi}{2}\ ||\ \ \theta < -\frac{\pi}{2} \\ -1\ , & \frac{\pi}{2}\ \geq\ \ \theta \geq\ -\frac{\pi}{2} \end{cases},$$

and

$$\zeta = \begin{cases} \frac{1}{8}\ , & f \leq 150 \\ \frac{1}{32}\ , & f > 150 \end{cases}.$$

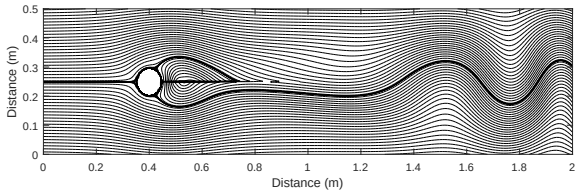
In Equation 35, $\left(\sin^2(\theta)+(\eta)^{\frac{-\frac{r^2}{4V_\infty^2 t^2}}{2}}\right)$ becomes a complex function depending on η which assumes positive unity in the windward face and negative unity in the leeward face, the sine term along with the real part of the complex η term damp the extent of the shedding away from the crests towards the center line of the cylinder, r^2 in the exponent curtails the field of the shedding at infinity and $4V_\infty^2 t^2$ extends the field of the shedding at the freestream velocity;
$\mathrm{e}^{-\left(\frac{125}{f_\infty}\right)}$ triggers the bifurcation at $f \sim 50$ using the exponential function in the form of a 'switch';
$r(t)$ convects the vortices with the flow and ;
$\mathrm{e}^{-\frac{130}{f_\infty}\left(\frac{r}{\sqrt{R^2+4\nu t}}-1\right)^2}$ ensures that the vortex shedding continues as its counterpart larger term dissipates at moderate to high f. This last term is modeled on the Batchelor vortex model[18] making Equation 35 a 'tribrid' Lamb-Oseen-Batchelor-Burgers vortex model.
Combining Equations 34 and 35 gives

$$\psi_{viscous} = \mathcal{R}\left(\psi_{NLF} + \psi_{vortex} + \psi_{sink/source} + \psi_{gravity} + \psi_{vortexshedding}\right). \tag{37}$$

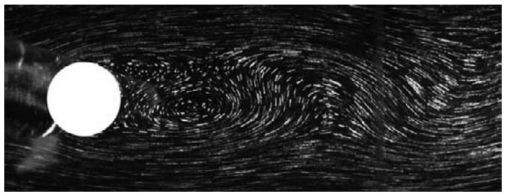
Figure 3 presents a qualitative comparison between the vortex shedding process predicted with Equation 37 (with an infinite domain) and the real process as photographed from a towing tank experiment[21].
Equipped with a viscous stream function, the velocity field becomes known and the unknown pressure field can be sought for.

A. Solution to the Navier-Stokes Equations

The compressible NSE are expressed in an equivalent differential form in Equation 38 using the compact vector form and with the role of vorticity made obvious through the application of some vector identities[17].



(a) Streamlines from the Present theory ($f = 100, t = 500s$)



(b) Instantaneous vortex shedding from the lower half of a circular cylinder at $f = 100$ ([21])

Figure 3: Comparison of counter-rotating vortex shedding behind the cylinder between the present theory and flow visualization from experiments conducted by Wu et al.[21]

$$\frac{\partial(\rho\mathbf{V})}{\partial t} + \nabla p + \rho\nabla\left(\frac{1}{2}V^2 + \mathbf{g}\cdot\mathbf{r}\right) = \rho\mathbf{V}\times\omega + \nabla\left((\lambda+\mu)\nabla\cdot\mathbf{V}\right) - \mu\nabla\times\omega \tag{38}$$

In keeping with the fore-running assumption of an incompressible flow, a solution to the NSE is sought in terms of the known stream function/ velocity components as expressed in Equation 39. However, a number of problems immediately arise. One of which is that the stream function in Equation 37 is two dimensional. Stream functions are usually difficult to define for general three dimensional space. Additionally, integrating the pressure out of this equation by vector identity manipulations is impossible due to the terms involving the vorticity and the local temporal derivative. Even though, Equation 37 is continuously differentiable in space and time, present mathematical methods even with the use of symbolic mathematical softwares like *Maple* do not offer anti-derivatives to such an involved equation. Numerical integration would not be in the spirit of solving the problem analytically but even when that is done, different results are obtained from integrating in either of the two spatial directions. Muriel[32] also encountered this problem and suggests that the pressure is a higher order tensor which converges to a scalar value in a long-time limit. However, everyday experience of pressure appears to suggest otherwise. A possible way out is to repeat the foregoing theoretical development in terms of the classical velocity potential which is well defined for three dimensional flows and would satisfy the unsteady Bernoulli equation in Equation 39 but it is mathematically undefined in the classical form as it is known for a rotational flow.

$$\begin{aligned}\rho\left(\nabla\times\frac{\partial\psi}{\partial t}\right) + \nabla\left(p + \frac{1}{2}\rho V^2 + \rho\mathbf{g}\cdot\mathbf{r}\right) &= \rho\mathbf{V}\times\omega + \nabla\left((\lambda+\mu)\nabla\cdot\mathbf{V}\right) - \mu\nabla\times\omega = \rho\mathbf{V}\times\omega - \mu\nabla\times\omega \\ \nabla\left(\rho\frac{\partial\phi}{\partial t} + p + \frac{1}{2}\rho V^2 + \rho\mathbf{g}\cdot\mathbf{r}\right) &= \rho\mathbf{V}\times\omega + \nabla\left((\lambda+\mu)\nabla\cdot\mathbf{V}\right) - \mu\nabla\times\omega = 0\end{aligned} \tag{39}$$

In his appraisal of vorticity, Saffman[12] points out the obvious that in dealing with real fluids in details the condition of irrotationality must be dropped. This essentially negates the physical existence of the classical velocity potential. But the presence of pressure as a scalar quantity and its physical relations to the velocity vector embodied in the NSE suggests a potential function for velocity for which a solution integrating away the vorticity to obtain the pressure as in Equation 40 exists.

$$\nabla\left(\rho\frac{\partial\kappa}{\partial t} + p + \frac{1}{2}\rho V^2 + \rho\mathbf{g}\cdot\mathbf{r} - (\lambda+\mu)\nabla^2\kappa\right) = 0 \tag{40}$$

Obtaining κ from Equation 37 in the cylindrical polar coordinate system still requires an integration process with brute force which is not supported by available modern mathematical methods. Realizing the

equivalence of coordinate systems, Equation 37 is recast in the cartesian coordinate system and the negative wind x-axis which is coincident with the negative body x-axis(horizontal and pointing to the left in Figure 3) is rotated an angle of $\frac{\pi}{2}$ clockwise to the positive body y-axis (vertical and pointing upwards in Figure 3). Essentially, the angle in Equation 37 is redefined as

$$\theta = \arctan(y, x) \Rightarrow \arctan(x, y) \ .$$

The freestream flow which is locked to the negative wind x-axis approaches from the positive body y-axis allowing for the function κ satisfying the continuity equation and Equation 40 to be defined with properties summarized in comparison to the classical velocity potential and the stream function in Table 1.

Table 1: Properties of the *Kwasu* function in comparison to the classical velocity potential and the stream function.

	ϕ	κ	ψ
V_r	$\frac{\partial \phi}{\partial r}$	$\frac{1}{r}\frac{\partial \kappa}{\partial \theta}$	$\frac{1}{r}\frac{\partial \psi}{\partial \theta}$
V_θ	$\frac{1}{r}\frac{\partial \phi}{\partial \theta}$	$-\frac{\partial \kappa}{\partial r}$	$-\frac{\partial \psi}{\partial r}$
V_z	$\frac{\partial \phi}{\partial z}$	$\frac{\partial \kappa}{\partial z}$	0
u	$\frac{\partial \phi}{\partial x}$	$\frac{\partial \kappa}{\partial x}$	$\frac{\partial \psi}{\partial y}$
v	$\frac{\partial \phi}{\partial y}$	$\frac{\partial \kappa}{\partial y}$	$-\frac{\partial \psi}{\partial x}$
w	$\frac{\partial \phi}{\partial z}$	$\frac{\partial \kappa}{\partial z}$	0
V_r	$u\cos\theta + v\sin\theta$	$-u\sin\theta + v\cos\theta$	$u\cos\theta + v\sin\theta$
V_θ	$-u\sin\theta + v\cos\theta$	$-(u\cos\theta + v\sin\theta)$	$-u\sin\theta + v\cos\theta$
V_z	$-(u\sin\theta - v\cos\theta)\cos\varphi$	$-(u\cos\theta + v\sin\theta)\cos\varphi$	0

The pressure which is a scalar quantity (zeroth order tensor) remains invariant to this rotation of axes. The operation carried out to obtain κ as expressed in Equation 41 is akin to finding the 'principal axis' for a rotational(viscous and real) flow about which the vorticity vector is identically zero even though the flow is really abound with vorticity concentrated towards the surface and in the wake. In this axis (which seems always aligned with the wind axis with its negative x-axis pointing into the incident flow), κ exists as a 'velocity potential' for both two and three dimensional real viscous flows.In the global cylindrical polar coordinate axis the orientation of which remains unchanged under this operation, κ satisfies the two dimensional instantaneous continuity equation identically and yields the component of the vorticity vector for the flow as standardly defined in this axis. In three dimensions, the κ field is not divergence-free because the spanwise third component of velocity is not constant along the z-axis $\frac{\partial V_z, w}{\partial z} \neq 0$. However, $\frac{\partial V_z, w}{\partial z}$ is observed to be an odd function about a plane parallel to the wind axis and with origin coincident with that of the body axis. Consequently, its volume integral over the entire space in keeping with the physical definition of the conservation of mass in Equation 1 is equal to zero for all times. Similarly, the integral of its contribution to the physical conservation of momentum as embodied in Equation 2 over the entire domain equals zero for all times.

Figure 4 shows the comparison between the predictions of the streamwise velocity component (u) calculated from ψ and κ. It is observable that both figures have excellent qualitative similarities even though there is a phase lag in temporal space between the two. Therefore, assuming $\mathbf{g} \cdot \mathbf{r}$ in Equation 40 (i.e. body forces including those due to electromaganetic fields e.t.c. These are not inclusive of gravity as it has already been incorporated into κ) is defined by a potential or identically equal to zero as allowed by Fefferman,[31] Equation 41 is integrable to obtain the pressure distribution which identically solves the incompressible NSE.

It is important to note that Equation 41 extends to all values of f and ν. However, dimensional analysis dictates that the aerodynamic forces are functions of both f and M amongst other variables[16]. Therefore, a solution to the compressible NSE (Equation 38) is sought. This is accomplished by incorporating the principle of conservation of energy embodied in the definition of the adiabatic speed of sound in Equation 42 along with the relations between pressure and density in Equation 43 into the definition of κ. This is the approach taken in deriving the full velocity potential equations[16] as well. The local velocity in these equations are obtained from the incompressible κ.

$$\kappa = V_\infty r\sin\theta_R\left(1-\frac{R^2}{r^2}\right) - V_\infty r\sin\theta_R\left(1+\frac{R^2}{r^2}\right)\ln\left(\frac{r}{R}\right)\mathrm{e}^{-\left(\frac{r^2}{V_\infty^2 t^2}+\frac{130(0.03061 f_\infty)^{\mathrm{e}^{\frac{10}{f_\infty}}}}{8f_\infty}\sqrt{\left(1-\frac{R^2}{r^2}\right)^2+4\,\frac{R^2\sin^2\theta_R}{r^2}}+2\left(\frac{r}{R}-1\right)\right)}$$

$$+V_\infty r\left(1-\frac{R^2}{r^2}\right)\ln\left(\frac{r}{R}\right)\left(\cos\theta_R-\frac{65\left(0.03061 f_\infty\right)^{\mathrm{e}^{\frac{10}{f_\infty}}}}{f_\infty}\,\frac{\sin^2\theta_R\cos\theta_R\left(\frac{r}{R}-1\right)\frac{R^2}{r^2}}{\sqrt{\left(1-\frac{R^2}{r^2}\right)^2+4\,\frac{R^2\sin^2\theta_R}{r^2}+2}}\right)$$

$$\left(\left(\theta_R\right)\chi\sin\left(\theta_R+\epsilon\right)\right)^{\mathrm{e}^{-\frac{\mathrm{a}_\infty \mathrm{t}}{\mathrm{r}}\left(1-\frac{\mathrm{R}}{\mathrm{r}}\right)}}\mathrm{e}^{-\left(\frac{r^2}{V_\infty^2 t^2}+\frac{130(0.03061 f_\infty)^{\mathrm{e}^{\frac{10}{f_\infty}}}}{8f_\infty}\sqrt{\left(1-\frac{R^2}{r^2}\right)^2+4\,\frac{R^2\sin^2\theta_R}{r^2}}+2\left(\frac{r}{R}-1\right)\right)}$$

$$+\frac{V_\infty}{\zeta}r\left(1-\frac{R^2}{r^2}\right)\ln\left(\frac{r}{R}\right)\left(\cos\theta_R-\frac{65\left(0.03061 f_\infty\right)^{\mathrm{e}^{\frac{10}{f_\infty}}}}{f_\infty}\,\frac{\sin^2\theta_R\cos\theta_R\left(\frac{r}{R}-1\right)\frac{R^2}{r^2}}{\sqrt{\left(1-\frac{R^2}{r^2}\right)^2+4\,\frac{R^2\sin^2\theta_R}{r^2}+2}}\right)\left(\left(\theta_R\right)\chi\sin\left(\theta_R+\epsilon\right)\right)^{\mathrm{e}^{-\frac{\mathrm{a}_\infty \mathrm{t}}{\mathrm{r}}\left(1-\frac{\mathrm{R}}{\mathrm{r}}\right)}}$$

$$\mathrm{e}^{-\left(\frac{125}{f_\infty}+\frac{r^2}{V_\infty^2 t^2}\right)-\left(\mathrm{e}^{-\frac{130}{f_\infty}\left(\frac{r}{\sqrt{R^2+4\nu t}}-1\right)^2+\frac{130(0.03061 f_\infty)^{\mathrm{e}^{\frac{10}{f_\infty}}}}{8f_\infty}\sqrt{\left(1-\frac{R^2}{r^2}\right)^2+4\,\frac{R^2\sin^2\theta_R}{r^2}}+2\left(\frac{r(t)}{R}-1\right)}\right)\left(\sin^2\left(\theta_R\right)+(\eta)^{\mathrm{e}^{-\frac{r^2}{4V_\infty^2 t^2}}}\right)}$$

$$+\frac{\mu_g\cos\left(\varphi-\frac{\pi}{2}\right)(t_\varrho-\mathcal{T})}{r}\left[1+\frac{3}{4}\left(\frac{R_B}{r}\right)^2+\frac{45}{64}\left(\frac{R_B}{r}\right)^4+\ldots\right], \tag{41}$$

where

$$r(t)=r\sqrt{\left(\sin\theta_R-\frac{V_\infty t}{r}\left(\frac{R^2}{r^2}\sin\theta_R\cos\theta_R\right)\right)^2+\left(\cos\theta_R-\frac{V_\infty t}{r}\left(1+\frac{R^2}{r^2}\left(\sin^2\theta_R-\cos^2\theta_R\right)\right)\right)^2},$$

$$\theta_R=\arctan\left[\left(x\cos\alpha-y\sin\alpha\right),\left(x\sin\alpha+y\cos\alpha\right)\right],$$

$$x=\left(r\cos\theta\cos\alpha-r\sin\theta\sin\alpha\right)\sin\left(\varphi+\beta\right),$$

$$y=\left(r\cos\theta\sin\alpha+r\sin\theta\cos\alpha\right)\sin\left(\varphi+\beta\right),$$

$$z=r\cos\left(\varphi+\beta\right),$$

$$r=\sqrt{x^2+y^2+z^2}$$

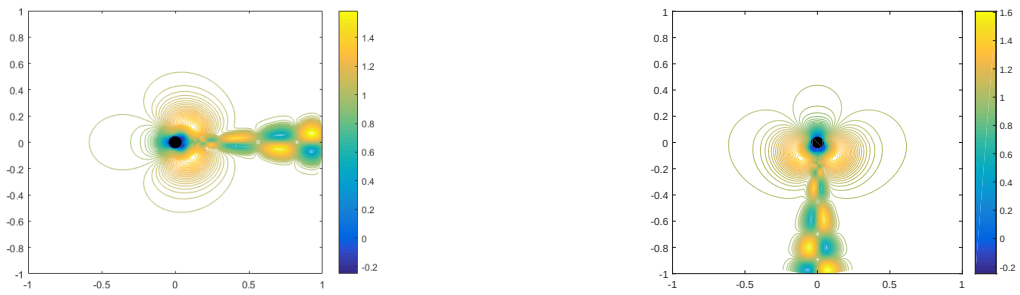
$$\eta=\begin{cases}1\ , & \theta_R>\frac{\pi}{2}\ ||\ \ \theta_R<-\frac{\pi}{2}\\ -1\ , & \frac{\pi}{2}\ \geq\ \ \theta_R\geq\ -\frac{\pi}{2}\end{cases},$$

$$\epsilon=\begin{cases}0.001\ , & \theta_R\geq 0\\ -0.001, & \theta_R<0\end{cases},$$

$$\chi=\begin{cases}1\ , & \theta_R\geq 0\\ -1\ , & \theta_R<0\end{cases},$$

and

$$\zeta=\begin{cases}\frac{1}{8}\ , & f\leq 150\\ \frac{1}{32}\ , & f>150\end{cases}.$$



(a) The velocity component along the flow direction (flow is from left to right), u, as obtained with Equation 37($f = 500, t = 1000s$)

(b) The velocity component along the flow direction (the flow is from top to bottom with $\alpha = 0$), u, as obtained with Equation 41($f = 500, t = 1000s$)

Figure 4: Comparison of the result of the integration of Equation 37 by rotation of cartesian coordinate axis about z-axis. There is a time shift after the rotation and both Equations 37 and 41 do not match exactly in the temporal space

$$a^2 = a_0^2 - \frac{\gamma - 1}{2} V^2 \tag{42}$$

$$dp = a^2 d\rho$$
$$dp = -\rho V dV = -\frac{\rho d(V^2)}{2} \tag{43}$$

Thus, Equation 44 is derived from the integration of the ensuing differential equation in ρ and V.

$$\frac{\rho}{\rho_\infty} = \left(\frac{1 - \frac{\gamma-1}{2} M_\infty^2}{1 - \frac{\gamma-1}{2} M^2} \right)^{\frac{1}{\gamma-1}} \tag{44}$$

With this, κ is redefined in its compressible form as

$$\kappa = Equation\ 44 \times Equation\ 41\ . \tag{45}$$

This satifies the physical principle of the conservation of mass in the entire domain embodied in the integral form of the continuity equation(Equation 1) in a similar manner as discussed for the incompressible version and noting that the volume integral of the transient variation of the density is zero assuming there are no reactions consuming or producing mass in the infinite domain. The condition of the wall velocity ($\alpha = \beta = 0, \varphi = \frac{\pi}{2}$) are

$$V_{r,w} = \frac{157 \mu_g (t_\varrho - \mathcal{T})}{64 R_B^2} \left[\frac{\partial \rho / \partial \theta}{\rho} + \frac{\partial (t_\varrho - \mathcal{T}) / \partial \theta}{(t_\varrho - \mathcal{T})} \right]_w ,$$

and

$$V_{\theta,w} = -2 V_\infty \sin\theta \left(1 - \mathrm{e}^{-\frac{R^2}{V_\infty^2 t^2}} \right) - \frac{\mu_g (t_\varrho - \mathcal{T})}{64 R_B^2} \left(157 R_B \left[\frac{\partial \rho / \partial r}{\rho} + \frac{\partial (t_\varrho - \mathcal{T}) / \partial r}{(t_\varrho - \mathcal{T})} \right]_w - 433 \right) . \tag{46}$$

Equation 46 is expository on the subject of the validity of the no-slip condition.The condition at the wall is transient and with a tendency from slip towards complete no-slip at some 'equilibrium' only when the freestream velocity is steady, the flow is assumed to be incompressible, the size of the body is relatively

super-large, the curvature of the body is negligible and the affinity between the fluid and the body is negligible. For a turbulent freestream flow, this equilibrium state may be unachievable since the 'relaxation time' towards this state is dependent on the instantaneous value of the freestream as Equation 46 suggests. This appears to be an alternative explanation to why Hoffman and Johnson[19,27] were successful in the computation of drag applying the slip condition to the turbulent computational solution of the NSE initialized with the classical potential flow solution. It also appears to dispel the idea that boundary layers do not exist in the solution of the NSE as they eventually concluded in their 2016 paper[27]. In fact, Figure 5 presents the velocity profiles obtained in the boundary layer at three different angular locations representative of attached, separating and separated flows as obtained from the present work. Here, the angle is measured from the front stagnation point. The boundary layer thickness was computed by solving the radial location for which the tangential velocity gradient becomes zero.

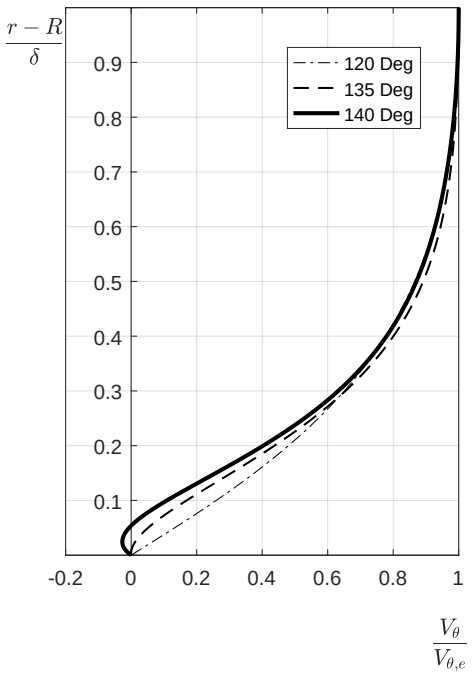


Figure 5: The velocity profile in the boundary layer at different stations (Present theory, $f = 26$,$\mathcal{M}_B = 1kg$,$R = 0.047$).

This figure represents the result for a steady freestream flow. It is suggestive that the '*sufficient*' conditions for the application of no-slip condition are incompressibility, steadiness, large body size, surface flatness e.t.c. as Equation 46 embodies. These agree with some of the observations which Brenner[1] reports.
The compressible pressure distribution in the entire space follows from Equation 47 with all its constituent components evaluated with Equation 45.

$$\nabla\left(\frac{\partial\kappa}{\partial t}+p+\frac{1}{2}\rho V^2+\rho\mathbf{g}\cdot\mathbf{r}-(\lambda+\mu)\,\nabla^2\kappa\right)=0 \tag{47}$$

Assuming the fluid is a perfect gas, the compressible temperature field is obtained as

$$T=\frac{p}{\rho R_g} \tag{48}$$

and the aerodynamic heat flux as

$$q=-k(x,y,z)\nabla T\ . \tag{49}$$

The perifocal stream function for the viscous flow over the circular cylinder is thus given as

$$\Psi = -h\frac{\rho}{\rho_\infty} \ . \tag{50}$$

The shear stress in the perifocal frame of reference is obtained as

$$\tau_{\varrho\Theta} = \mu\left(\frac{\partial V_\Theta}{\partial \varrho} - \frac{V_\Theta}{\varrho} + \frac{1}{\varrho}\frac{\partial V_r}{\partial \Theta}\right) = \mu\left(\frac{\partial V_\Theta}{\partial r} - \frac{V_\Theta}{\varrho} + \frac{1}{\varrho^2 V_\Theta}\mu_g \epsilon \cos\Theta\right) \ . \tag{51}$$

When this is evaluated and set equal to zero, the true anomaly at separation is obtained as

$$\Theta_s = \cos^{-1}\left[\left(\frac{-\varrho^2(V_\theta\frac{\partial V_\theta}{\partial r} + V_z\frac{\partial V_z}{\partial r} - \frac{V_z^2+V_\theta^2}{\varrho})}{\mu_g\sqrt{1+\frac{h^2}{\mu_g^2}\left(V^2 - \frac{2\mu_g}{\varrho}\right)}}\right)_{\varrho=r=R,\theta=\pm\pi}\right] . \tag{52}$$

At the onset of transition to turbulence in the boundary layer, there is a divergence in the value of the surface shear stress. The transition point is thus obtained at the point where the circumferential derivative of the perifocal shear stress tends towards infinity. Examination of Equation 51 indicates that this point occurs when h tends to zero at which point

$$\Theta_{Tr} = \cos^{-1}\left[\left(-\frac{1}{\varepsilon}\right)_{\varrho=r=R,\theta=\pm\pi}\right] . \tag{53}$$

In order to reference quantities in the perifocal frame to the body axis the following orbital elements are obtained as[35]

$$\varphi_i = \cos^{-1}\left(\frac{h_z}{h}\right) , \tag{54}$$

$$V_\varrho = \frac{(xu + yv + zw)}{r} \ , \tag{55}$$

$$\Omega = \cos^{-1}\left[\frac{h_y}{\sqrt{h_x^2 + h_y^2}}\right] , \tag{56}$$

$$\Upsilon = \cos^{-1}\left[\frac{\frac{h_y}{\mu_g}\left[\left(V^2 - \frac{\mu_g}{r}\right)x - rV_\varrho u\right] - \frac{h_x}{\mu_g}\left[\left(V^2 - \frac{\mu_g}{r}\right)y - rV_\varrho v\right]}{\sqrt{\left(h_x^2+h_y^2\right)\left(1+\frac{h^2}{\mu_g^2}\left(V^2 - \frac{2\mu_g}{r}\right)\right)}}\right] \ , \tag{57}$$

and

$$\{\mathbf{r}\}_{\tilde{x}} = \frac{h^2}{\mu_g}\frac{1}{1+\varepsilon\cos\Theta}\left\{\begin{array}{c}\cos\Theta\\ \sin\Theta\\ 0\end{array}\right\} . \tag{58}$$

The Euler angle matrix for the transformation between the body perifocal frame to the body axis is then given as

$$[\mathbf{Q}]_{\tilde{x}x} = \begin{bmatrix} -\sin\Omega\cos\varphi_i\sin\Upsilon + \cos\Omega\cos\Upsilon & -\sin\Omega\cos\varphi_i\cos\Upsilon - \cos\Omega\sin\Upsilon & \sin\Omega\sin\varphi_i \\ \cos\Omega\cos\varphi_i\sin\Upsilon + \sin\Omega\cos\Upsilon & \cos\Omega\cos\varphi_i\cos\Upsilon - \sin\Omega\sin\Upsilon & -\cos\Omega\sin\varphi_i \\ \sin\varphi_i\sin\Upsilon & \sin\varphi_i\cos\Upsilon & \cos\varphi_i \end{bmatrix} , \tag{59}$$

so that the position vector with respect to the body axis is obtained as

$$\{\mathbf{r}\}_x = [\mathbf{Q}]_{\tilde{x}x}\{\mathbf{r}\}_{\tilde{x}} \, . \tag{60}$$

Hence the separation and transition points are located on the cylindrical surface as

$$\theta_s = \tan^{-1}\left[\frac{\sin\Omega\cos\left(\Upsilon+\Theta_s\right) + \cos\Omega\sin\left(\Upsilon+\Theta_s\right)\cos\varphi_i}{\cos\Omega\cos\left(\Upsilon+\Theta_s\right) - \sin\Omega\sin\left(\Upsilon+\Theta_s\right)\cos\varphi_i}\right] , \tag{61}$$

and

$$\theta_{Tr} = \tan^{-1}\left[\frac{\sin\Omega\cos\left(\Upsilon+\Theta_{Tr}\right) + \cos\Omega\sin\left(\Upsilon+\Theta_{Tr}\right)\cos\varphi_i}{\cos\Omega\cos\left(\Upsilon+\Theta_{Tr}\right) - \sin\Omega\sin\left(\Upsilon+\Theta_{Tr}\right)\cos\varphi_i}\right] . \tag{62}$$

With the foregoing, the complete three dimensional unsteady compressible flow field around the cylinder in an infinite domain has been presented. The expression for the velocity field obtained from κ exhibit a singularity only at $t = 0$. Therefore the use of an absolute $t = 0$ in the equation is discarded. There is physical credence to holding this position as the local time in reality is a relative quantity. Since, the velocity field is continuous in every relative time and everywhere in the flow field, and since the freestream is recovered in the limit as $r \to \infty$ as well as for the fact that Fefferman[31] allows for a spatially periodic solution such as is the case in the predicted wake, it is stated with no proof that the energy of the foregoing solution to the NSE is bounded. Again, it is noted that the foregoing work, though focused on the circular cylinder to make the presentation here tractable, is extendibles to the general case of the solution of the Laplace equation in Equation 5 for which $m \geq 1$ and summations of these terms thereof. In this manner, complete analytical solutions to the flow field around arbitrary geometries may be realizable. Indeed, with the use of suitable conformal maps (both analytical such as presented in Equation 63[29] and numerical), the specific treatment here for $m = 1$ can be mapped to other geometries. The quantitative analysis of the results presented here as well as for such other geometries as will be studied are subjects of planned future work.

$$l = \frac{(a^2 - b^2)^{\frac{1}{2}}}{2}$$

$$r = \sqrt{[lexp(\cosh^{-1}\mathcal{P})]^2 + z^2}$$

$$\theta = \tan^{-1}\left(\frac{y}{x}\frac{\mathcal{P}}{[\mathcal{P}^2 - 1]^{\frac{1}{2}}}\right)$$

$$R = \sqrt{(a^2\cos^2\theta + b^2\sin^{\theta} + z^2)}$$

$$\mathcal{P} = \left[\frac{\frac{x^2}{l^2} + \frac{y^2}{l^2} + 4 + \left(\left[\frac{x^2}{l^2} + \frac{y^2}{l^2} + 4\right]^2 - \frac{16x^2}{l^2}\right)^{\frac{1}{2}}}{8}\right]^{\frac{1}{2}} .$$

(63)

B. High Reynolds Number Compressible Turbulent Flows

Finally, to the subject of most significance in fluid dynamics: Turbulence. It is conjectured until further investigation that the turbulence in the flow field predicted using κ may be tracked by computing the entropy field of the flow using its relation to temperature and pressure as presented in standard fluid dynamics and thermodynamics texts. Regions of observable largely increased entropy would be identified as indicative of the chaos and randomness of turbulence. Muriel found no promise of turbulence to the disappointment of the mathematics and physics community in his proposed solution to the NSE as formulated by CMI and conjectures against the possible thrust of the present work that no solution to the NSE will exhibit turbulence. He faulted this on the inappropriate basement of the Navier-Stokes on the continuum model.[32] He notes, and the current author agrees, that turbulence may be due to the "internal degrees of freedom to be found in atoms and molecules with excitable quantum states"[33]. The present formulation presents a unified framework to attempt a theoretical simulation and/or prediction of turbulence incorporating Muriel's submission. In performing this analysis, it will be important to note that

- real surfaces are rough and not as smooth as described by the assumption of a constant R in this formulation. Such roughness may even be a function of time as the flow progresses and the surface erodes. Any detailed attempt to tracking turbulence will have to take uneven surfaces into account.
- all freestream properties employed as well as geometric position variables may also be functions of time.
- the thermodynamic quantities employed will have to accomodate equations which take the changes in the internal energies of the atoms and molecules into account as suggested by Muriel.
- a useful strategy will be taking a chronological approach to modeling the non-linear temporal coupling of all these variables starting by computing a variable which may precede the onset of the change in another at a specific time step and using the final value of the last variable in the chronological sequence to predict the value of the antecedent variables in the next time step.

Such computations are planned for future studies and reporting.

V. Conclusion

Classical inviscid theory of the steady flow over obstacles falls short of resolving real flow phenomena brought about by the fluid viscosity and results in the d'Alembert's paradox. This is because the physics of the real flow is governed by the non-linear Navier-Stokes equation which have persistently resisted a general analytic solution. Adequate numerical solutions of the Navier-Stokes equation provide results matching closely with experiments. However, such computations are costly and time-consuming depending on geometric complexity and Reynolds number amongst other things. Therefore, a refinement of the classical theory which provides realistic results would be most useful.

In the present work, a closed form analytic solution to the complete unsteady compressible Navier-Stokes equation in the form of a scalar function,*Kwasu* function, is presented. Preliminary results of the work show that the theory presented captures important features of a bluff body flow including flow separation, wake formation, vortex shedding as well as compressibilty effects. Qyantititative analysis of these results will be made in further studies.

The condition at a viscous wall is shown to be transient between the slip and no-slip limits. It is the hope that the present theory will shed more light on the important phenomenon of turbulence in planned future work.

Acknowledgments

The author would like to acknowledge and appreciate the Almighty God for the inspiration for and the supervision of this study as well as Kwara State University, Malete, Nigeria for the financial support of the author's post graduate studies at Georgia Institute of Technology (GATECH), Atlanta, US. The comments of Professor Marilyn J. Smith of the Non-Linear Computational Aeroelasticity Laboratory, GATECH who is the author's advisor and those of Nicholson Koukpaizan, a fellow PhD candidate, are very acknowledged and highly appreciated.

References

[1]Brenner, Howard, *Beyond the no-slip boundary condition*, Physical Review, 2011.
[2]D'Alessio, S. J. D.; Dennis, S. C. R., *A Vorticity Model for Viscous Flow Past a Cylinder*, Computers Fluids, 1994.
[3]Day, Michael A., *The No-Slip Condition Of Fluid Dynamics*, Erkenntnis, 1990.
[4]Fornberg, Bengt, *Steady Viscous Flow Past a Circular Cylinder*, Journal Of Computational Physics, 1985.
[5]Gautier, R.; Biau, D.; Lamballais, E., *A reference solution of the flow over a circular cylinder at Re = 40*, Computers and Fluids, 2013.
[6]Hafez, Mohamed; Wahba, Essam, *Inviscid flows over a cylinder*, Comput. Methods Appl. Mech. Engrg., 2004.
[7]Jain, P. C.; Goel, B. S., *Shedding Of Vortices Behind a Circular Cylinder*, Computers and Fluids, 1976.
[8]Niemann, H.-J.; Holscher, N., *A Review of Recent Experiments on the Flow past a Circular Cylinder*, Journal of Wind Engineering and Industrial Aerodynamics, 1990.
[9]Nieuwstadt, F.; Keller, H. B., *Viscous Flow Past Circular Cylinders*, Computers and Fluids, 1973.
[10]Patel, V. A., *Karman Vortex Street behind a Circular Cylinder by the Series Truncation Method*, Journal of Computational Physics, 1978.
[11]Patel, V. A., *Symmetry of the Flow around a Circular Cylinder*, Journal of Computational Physics, 1987.
[12]Saffman, P. G., *Dynamics of vorticity*, Journal of Fluid Mechanics, 1981.
[13]Stewartson, Keith, *D'Alembert's Paradox*, SIAM Review, 1981.
[14]Tuann, Shih-Yu; Olson, Mervyn D., *Numerical Studies of the flow around a Circular Cylinder by a Finite Element Method*, Computers and Fluids, 1978.
[15]Zhu, Yingxi; Granick, Steve, *Limits of the Hydrodynamic No-Slip Boundary Condition*, Physical Review Letters, 2002.
[16]Anderson, John D., *Fundamentals of Aerodynamics*, 5th Edition, McGraw-Hill, 2011.
[17]White, Frank M., *Viscous Fluid Flow*, 3rd Edition, McGraw-Hill,2006.
[18]Wu,J.-Z.; Ma,H.-Y.; Zhou, M.-D., *Vorticity and Vortex Dynamics*,2006.
[19]Hoffman, Johan; Johnson, Claes, *Resolution of d'Alembert's Paradox*, Journal Of Mathematical Fluid Mechanics, 2008.
[20]Zdravkovich, M. M., *Flow Around Circular Cylinders Volume 1: Fundamentals*, Oxford Science Publications, 1997.
[21]Wu, Ming-Hsun; Wen, Chih-Yung; Yen, Ruey-Hor; Weng, Ming-Cheng; Wang, An-Bang, *Experimental and numerical study of the separation angle for flow around a circular cylinder at low Reynolds number*, Journal Of Fluid Mechanics, vol. 515, pp. 233-260, Cambridge University Press, 2004.
[22]Sen, Subhankar; Mittal, Sanjay; Biswas, Gautam, *Steady separated flow past a circular cylinder at low Reynolds numbers*, Journal Of Fluid Mechanics, vol. 620, pp. 89-119, Cambridge University Press, 2009.
[23]Dennis, S.C.R.; Shimshoni, M, *The Steady Flow of a Viscous Fluid past a Circular Cylinder*,C.P. No.797, Aeronautical Research Council, Ministry of Aviation, London ,1965.
[24]Pope, Stephen B., *Turbulent Flows*, Cambridge University Press.
[25]Wilczek, M.; Jenko, F;Friedrich,R., *Lagrangian Particle Statistics in Turbulent Flows from a Simple Vortex Model*,DOI: 10.1103/PhysRevE.77.056301, arXiv:0707.0440,2007.
[26]Mouri, H.; Hori, A;Kawashima,Y., *Vortex tubes in velocity fields of laboratory isotropic turbulence: dependence on the Reynolds number*,DOI: 10.1103/PhysRevE.67.016305, arXiv:physics/0211044,2014.
[27]Hoffman, Johan; Jansson, Johan; Johnson, Claes, *New theory of Flight*, Journal Of Mathematical Fluid Mechanics 18,pp.219-241, 2016, DOI 10.1007/s00021-015-0220-y.
[28]Tazzioli, Rossana, *D'Alembert's paradox, 1900-1914: Levi-Civita and his Italian and French followers*, Comptes Rendus Mecanique 345,pp.488-497, 2017.
[29]Fitzpatrick,Richard, *Theoretical Fluid Mechanics*, The University of Texas at Austin, http://farside.ph.utexas.edu/teaching/336L/Fluidhtml/node87.html,2016-03-31.
[30]Fitzpatrick,Richard, *An Introduction to Celestial Mechanics*, The University of Texas at Austin.
[31]Feffermann,Charles L., *Existence and Smoothness of the Navier-Stokes*, The Clay Mathematics Institute of Cambridge Massachussets, url :http://www.claymath.org/millennium-problems/navier
[32]Muriel, A, *An exact solution of the 3-D Navier-Stokes equation*, Results in Physics 1,pp.2-8, 2011.
[33]Muriel, A, *Exact Solutions of the Navier-Stokes Equation as Subsets of Time Evolution Equations*, Technical report,Program in Mathematics, Graduate Center, City University of New York, 2015.
[34]Pines, Samuel, *Uniform Representation of the Gravitational Potential and its Derivatives*, AIAA Journal Vol. 11,No.11,pp.1508-1511, November 1973.
[35]Curtis, Howard D., *Orbital Mechanics for Engineering Students*, Elsevier Aerospace Engineering Series, 2005.
[36]Shapiro, Ascher H., *Bath-Tub vortex*, Physics, Nature, No.4859,pp.1080=1081, Nature Publishing Group, December 15, 1962.
[37]Barbagallo, John, *Aircraft Wake Turbulence*, Advisory Circular, U.S. Department of Transportation, Federal Aviation Administration, AC No:90-23G, 2014.